MUNC18-1 regulates the submembrane F-actin network, independently of syntaxin1 targeting, via hydrophobicity in -sheet 10

Pons-Vizcarra, Maria; Kurps, Julia; Tawfik, Bassam; Sørensen, Jakob B.; van Weering, Jan R.T.; Verhage, Matthijs

published in
Journal of cell science
2019

DOI (link to publisher)
10.1242/jcs.234674

document version
Publisher's PDF, also known as Version of record

© 2019. Published by The Company of Biologists Ltd | Journal of Cell Science (2019) 132, jcs242552. doi:10.1242/jcs.242552

CORRECTION

Correction: MUNC18-1 regulates the submembrane F-actin network, independently of syntaxin1 targeting, via hydrophobicity in β-sheet 10 (doi:10.1242/jcs.234674)

Maria Pons-Vizcarra, Julia Kurps, Bassam Tawfik, Jakob B. Sørensen, Jan R. T. van Weering and Matthijs Verhage

There was an error in *J. Cell Sci.* (2019) **132**, jcs234674 (doi:10.1242/jcs.234674).

The merge panels in Fig. 1G were inadvertently duplicated. The corrected and original panels are shown below; both the online full text and PDF versions of the paper have been corrected. The authors apologise to readers for this error, which does not impact the results or conclusions of the paper.

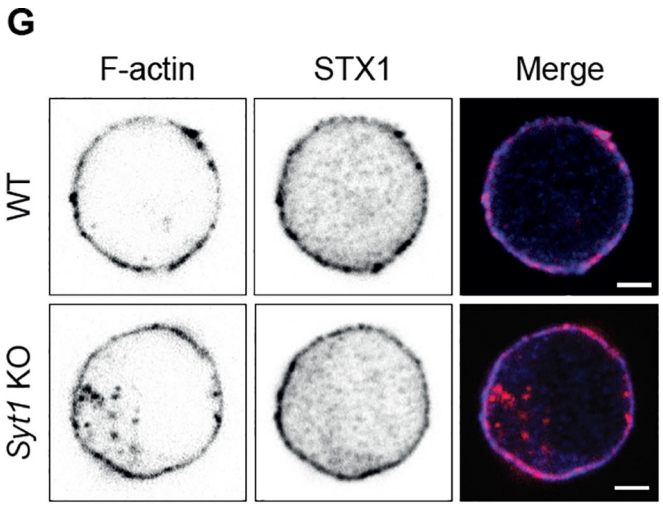

Fig. 1G (corrected panel). Increased F-actin network levels and STX1 mistargeting are phenotypes specific for *Munc18-1*-KO MCCs. (G) Confocal images of WT MCCs and *Syt1*-KO MCCs labeled with Rhodamine–phalloidin staining F-actin (first column) and STX1 staining (second column). The third column shows the merge of both signals. Scale bars: 2 µm.

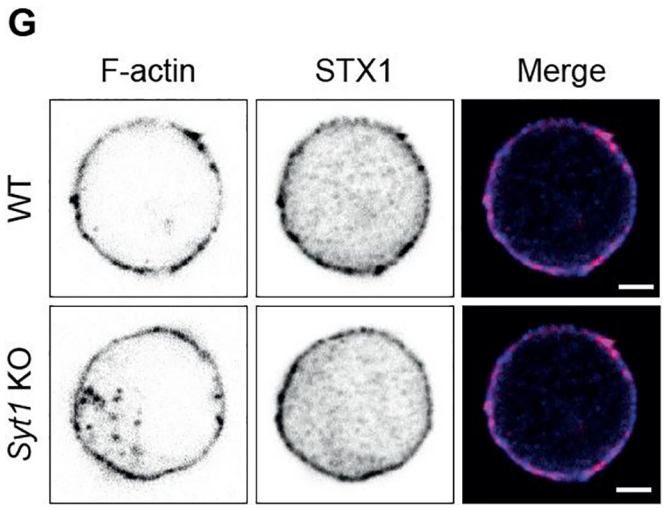

Fig. 1G (original panel). Increased F-actin network levels and STX1 mistargeting are phenotypes specific for *Munc18-1*-KO MCCs. (G) Confocal images of WT MCCs and *Syt1*-KO MCCs labeled with Rhodamine–phalloidin staining F-actin (first column) and STX1 staining (second column). The third column shows the merge of both signals. Scale bars: 2 µm.

© 2019. Published by The Company of Biologists Ltd | Journal of Cell Science (2019) 132, jcs234674. doi:10.1242/jcs.234674

RESEARCH ARTICLE

MUNC18-1 regulates the submembrane F-actin network, independently of syntaxin1 targeting, via hydrophobicity in β-sheet 10

Maria Pons-Vizcarra[1,*], Julia Kurps[1,*], Bassam Tawfik[2], Jakob B. Sørensen[2], Jan R. T. van Weering[3] and Matthijs Verhage[1,3,‡]

ABSTRACT

MUNC18-1 (also known as STXBP1) is an essential protein for docking and fusion of secretory vesicles. Mouse chromaffin cells (MCCs) lacking MUNC18-1 show impaired secretory vesicle docking, but also mistargeting of SNARE protein syntaxin1 and an abnormally dense submembrane F-actin network. Here, we tested the contribution of both these phenomena to docking and secretion defects in MUNC18-1-deficient MCCs. We show that an abnormal F-actin network and syntaxin1 targeting defects are not observed in *Snap25*- or *Syt1*-knockout (KO) MCCs, which are also secretion deficient. We identified a MUNC18-1 mutant (V263T in β-sheet 10) that fully restores syntaxin1 targeting but not F-actin abnormalities in *Munc18-1*-KO cells. MUNC18-2 and -3 (also known as STXBP2 and STXBP3, respectively), which lack the hydrophobic residue at position 263, also did not restore a normal F-actin network in *Munc18-1*-KO cells. However, these proteins did restore the normal F-actin network when a hydrophobic residue was introduced at the corresponding position. *Munc18-1*-KO MCCs expressing MUNC18-1(V263T) showed normal vesicle docking and exocytosis. These results demonstrate that MUNC18-1 regulates the F-actin network independently of syntaxin1 targeting via hydrophobicity in β-sheet 10. The abnormally dense F-actin network in *Munc18-1*-deficient cells is not a rate-limiting barrier in secretory vesicle docking or fusion.

This article has an associated First Person interview with the first author of the paper.

KEY WORDS: Docking, F-actin, MUNC18-1, MUNC18-2, MUNC18-3, Neuroendocrine, SM proteins, Secretion

INTRODUCTION

Neuronal and neurosecretory cell communication depends on the exocytosis of signaling molecules stored in secretory vesicles. Chromaffin cells are a model system widely used to study regulated vesicle secretion as their release machinery is similar to synaptic vesicles in neurons (Morgan and Burgoyne, 1997; Neher, 2018; Rettig and Neher, 2002). Moreover, the spatially distributed docking sites, where secretory vesicles attach to the plasma membrane (PM) prior to fusion, make these cells an attractive model to study secretory vesicle docking and fusion mechanisms (Verhage and Sørensen, 2008). However, the molecular organization of such docking sites is still incompletely defined.

Several proteins and lipids have been established as components of docking sites (for reviews, see Lauwers et al., 2016; Malacombe et al., 2006; Porat-Shliom et al., 2013; Südhof and Rizo, 2011; Verhage and Sørensen, 2008). MUNC18-1 (also known as STXBP1), a member of the Sec/MUNC18 (SM) protein family, is one of the essential proteins for regulated secretion in neurons and mouse chromaffin cells (MCCs), and without MUNC18-1, secretory vesicle docking is impaired in MCCs (Toonen et al., 2006; Verhage et al., 2000; Voets et al., 2001). In addition, *Munc18-1*-knockout (KO) MCCs have increased F-actin levels and a more-intact cortical F-actin network (Kurps and De Wit, 2012; Toonen et al., 2006) and ∼50% reduced syntaxin1 (STX1, note both STX1A and STX1B are expressed in MCCs) levels (Voets et al., 2001). Like MUNC18-1, STX1 is essential for vesicle docking and exocytosis in MCCs (de Wit et al., 2006), and STX1 targeting to the PM is impaired in *Munc18-1*-KO chromaffin cells (Gulyas-Kovacs et al., 2007). The contribution of these two null mutant phenotypes, altered F-actin and impaired STX1 targeting, to the docking defect in *Munc18-1*-KO MCCs is unknown.

Actin is expressed in most eukaryotic cells and contributes to many cellular processes, including vesicle trafficking. In the cortical regions underneath the PM of chromaffin cells, a dense F-actin network is the main component of the cytoskeleton (Cheek and Burgoyne, 1986). Two opposite roles have been described for F-actin: promoting vesicle transport (Gimenez-Molina et al., 2018; Lang et al., 2000; Trifaró et al., 2008) and preventing organelles, including vesicles, from reaching the PM (Toonen et al., 2006; Vitale et al., 1995, 1991). Actin filaments are dynamic and showed a stimulation-dependent polymerization that has been suggested to facilitate regulated exocytosis (Trifaró et al., 1992; Vitale et al., 1991). In bovine chromaffin cells, it seems that dynamin2 is necessary for actin reorganization (González-Jamett et al., 2013). Recently, it has been described that F-actin regulates the formation of the fusion pores in bovine chromaffin cells (Shin et al., 2018). It has also been shown that the relaxation of the F-actin network after stimulation might facilitate synaptic vesicle mobilization to the PM (Papadopulos et al., 2015). Indeed, destabilizing the cortical F-actin network in *Munc18-1*-KO cells restored morphological docking (Toonen et al., 2006), indicating that F-actin abnormalities may also contribute to the observed docking defect.

[1]Department of Functional Genomics, Center for Neurogenomics and Cognitive Research, Neuroscience Campus Amsterdam, Vrije Universiteit Amsterdam, de Boelelaan 1085, Amsterdam 1081 HV, The Netherlands. [2]Neurosecretion group, Signaling Laboratory, Department of Neuroscience and Pharmacology, University of Copenhagen, DK-2200 Copenhagen N, Denmark. [3]Department of Clinical Genetics, Center for Neurogenomics and Cognitive Research, Neuroscience Campus Amsterdam, Amsterdam UMC, location VUmc, de Boelelaan 1085, Amsterdam 1081 HV, The Netherlands.
*These authors contributed equally to this work

‡Author for correspondence (matthijs@cncr.vu.nl)

M.PV., 0000-0001-5008-5741; J.K., 0000-0002-8541-4151; B.T., 0000-0003-1193-8494; J.B.S., 0000-0001-5465-3769; J.R.T.v.W., 0000-0001-5259-4945; M.V., 0000-0002-6085-7503

Received 21 May 2019; Accepted 1 November 2019

Journal of Cell Science (2019) 132, jcs234674. doi:10.1242/jcs.234674

In this study, we assess the contribution of STX1 targeting and F-actin network distribution in the MUNC18-1-dependent secretory pathway. We confirm the previously reported increase in cortical F-actin and mistargeting of STX1, and show that this phenotype is specific for MUNC18-1 and not observed in other KO mutants with a docking and secretion defect. We identify a MUNC18-1 mutant, V263T, which does not rescue F-actin abnormalities in *Munc18-1*-KO MCCs, but fully restores STX1 targeting, showing that these phenotypes are independently regulated by MUNC18-1. MUNC18-2 and MUNC18-3 (also known as STXBP2 and STXBP3, respectively), lack a similar hydrophobic residue and fail to restore a normal F-actin network in *Munc18-1*-KO MCCs. When a hydrophobic residue was introduced, MUNC18-2 and -3 mutants do, indicating that this hydrophobic residue is necessary and sufficient for SM proteins to regulate F-actin. MUNC18-1(V263T) fully restored docking and secretion in *Munc18-1*-KO MCCs. Hence, we conclude that the increased cortical F-actin does not act as a rate-limiting factor for docking and secretion, and that F-actin network and STX1 targeting are independently regulated by MUNC18-1.

RESULTS

F-actin and STX1 phenotypes are MUNC18-1 specific and not explained by a docking deficiency alone

To test the role of the cortical F-actin network in docking and secretion in *Munc18-1* wild-type (WT) and KO MCCs, we first assessed the F-actin network using Rhodamine–phalloidin labeling. Labeling was quantified using the automated image analysis tool PlasMACC (Kurps et al., 2014) in WT and KO cells, and KO cells overexpressing WT MUNC18-1. Fig. 1A,D,G shows typical examples of the different conditions tested. *Munc18-1*-KO cells showed a ∼90% increase in F-actin ring intensity compared to WT MCCs (1.99±0.18 versus 1.00±0.06) (Fig. 1A,B), in line with previous observations (Toonen et al., 2006). Expression of MUNC18-1 WT on the KO background restored F-actin intensity to almost wild-type levels (1.36±0.11).

The cellular distribution of endogenous STX1 was analyzed through immunofluorescence and quantified as the ratio between PM and cytosolic labeling. As described previously (Munch et al., 2016), targeting of STX1 was impaired in the absence of MUNC18-1. The PM:cytosolic ratio was decreased by 50% in KO cells of *Munc18-1* (1.14±0.03 versus WT cells: 2.29±0.09, Fig. 1C). This WT ratio was almost completely restored with the acute expression of MUNC18-1 in KO cells (1.84±0.06, Fig. 1C). Hence, we confirmed that cortical F-actin levels are increased and STX1 is mistargeted in *Munc18-1*-KO cells and that these phenotypes are rescued by acute MUNC18-1 expression.

Docking is impaired in synaptosomal nerve-associated protein 25 (*Snap25*) and synaptotagmin1 (*Syt1*)-KO MCCs (de Wit et al., 2009). To assess whether the increased cortical F-actin and STX1 mistargeting are common features of cells that have docking defects, F-actin intensity and STX1 targeting were analyzed in MCCs from *Snap25*-KO and *Syt1*-KO mice (Fig. 1D,G). Cortical F-actin intensity at the PM in WT cells (1.0±0.06) and *Snap25*-KO (1.03±0.07) (Fig. 1E) were not significantly different. Similar results were obtained for *Syt1*-KO cells (0.99±0.05) compared to WT (1.0±0.04) (Fig. 1H). Similarly, no significant differences were observed in the targeting of STX1 in *Snap25*- and *Syt1*-KO cells compared to WT (PM:cytosolic ratio in WT of 1.77±0.08; 1.90±0.06; in KO of 1.58 ±0.07; 1.87±0.06; Fig. 1F,I). These results show that altered F-actin intensity and STX1 targeting are not a common feature of docking-impaired MCCs; thus impairment in docking is not sufficient to induce an increase in cortical F-actin. Instead, increased F-actin intensity and STX1 mistargeting are a consequence of the loss of MUNC18-1 specifically.

The majority of MUNC18-1 mutants tested support both a normal F-actin network and STX1 targeting

We aimed to map the F-actin network and STX1-targeting functions of MUNC18-1 to specific domains or residues by screening a collection of MUNC18-1 mutants in *Munc18-1*-KO MCCs and analyzing the F-actin network and STX1 PM:cytosolic ratios (Fig. 2; Table S1). Mutations at position Y473 and S241 are phosphorylation sites for different kinases: Y473 for Src kinase (Meijer et al., 2018) and S241 for extracellular signal-regulated kinases (ERKs) (Schmitz et al., 2016). Furthermore, we examined a group of MUNC18-1 mutations at positions where SM proteins that support synchronous release of synaptic vesicles (MUNC18-1, Rop and Unc18) are different from SM-proteins that do not (MUNC18-2 and MUNC18-3). These sites might be involved in a joint function of MUNC18-1 and MUNC13-1 in preventing de-priming (He et al., 2017). A summary of all the mutations used, the rationale for each mutation and their location are listed in Table S1. Typical examples of cells expressing the different mutants are shown in Fig. 2A. The expression of most MUNC18-1 mutants in *Munc18-1*-KO MCCs resulted in similar levels of F-actin intensity to that of MUNC18-1 WT (Fig. 2B). None of the mutants showed a reduced STX1 targeting ratio (Fig. 2C). However, the MUNC18-1(V263T) mutant failed to reduce the increased F-actin intensity (1.95±0.18, Fig. 2A,B), while restoring STX1 targeting as well as WT MUNC18-1 (1.85±0.08; Fig. 2C). In summary, this screen shows that the majority of mutants tested restore both F-actin intensity and STX1 targeting as well as WT MUNC18-1, but one mutation, MUNC18-1(V263T), produces a selective defect in restoring normal F-actin intensity.

MUNC18-1(V263T) supports STX1 targeting but not the regulation of the F-actin network

After the initial screening, we first quantitatively verified in separate experiments the F-actin intensity and STX1-targeting capacities of MUNC18-1(V263T) (Fig. 3). Typical examples of the different conditions tested are shown in Fig. 3A. In line with the experiments above, *Munc18-1*-KO MCCs showed a robust increase of F-actin labeling compared to WT (2.03±0.15 and 1.0±0.05, respectively). eGFP lentivirus was used as a control for the virus infection in both WT (1.04±0.11) and KO cells (1.97±0.17). No significant differences between the non-transfected and transfected cells were observed. Expression of MUNC18-1(V263T) did not restore F-actin levels (2.18±0.21), while expressing MUNC18-1 WT in MCCs cultured from the same animal fully restored F-actin levels (1.16±0.1; Fig. 3B). Conversely, MUNC18-1(V263T) restored the STX1 targeting (ratio 1.88±0.11) to a very similar extent to MUNC18-1 WT (ratio 1.9±0.09), and to a level comparable to the WT plus eGFP condition (ratio 1.92±0.1). These experiments confirm that MUNC18-1(V263T) restores STX1 targeting but not the changes in F-actin cytoskeleton, suggesting that MUNC18-1 regulates the F-actin network and STX1 targeting via distinct mechanisms.

F-actin network is restored by different SM proteins in the absence of MUNC18-1

The SM protein family is evolutionarily well conserved (Toonen and Verhage, 2003). We aligned several SM proteins to the residue 263 of MUNC18-1 (Fig. 4A), mutation of which failed to support a normal F-actin network. The location of the mutation V263T in the MUNC18–STX1 complex is shown in Fig. 4B. Kurps and De Wit (2012) showed a pilot experiment suggesting that *C. elegans* Unc18

Journal of Cell Science (2019) 132, jcs234674. doi:10.1242/jcs.234674

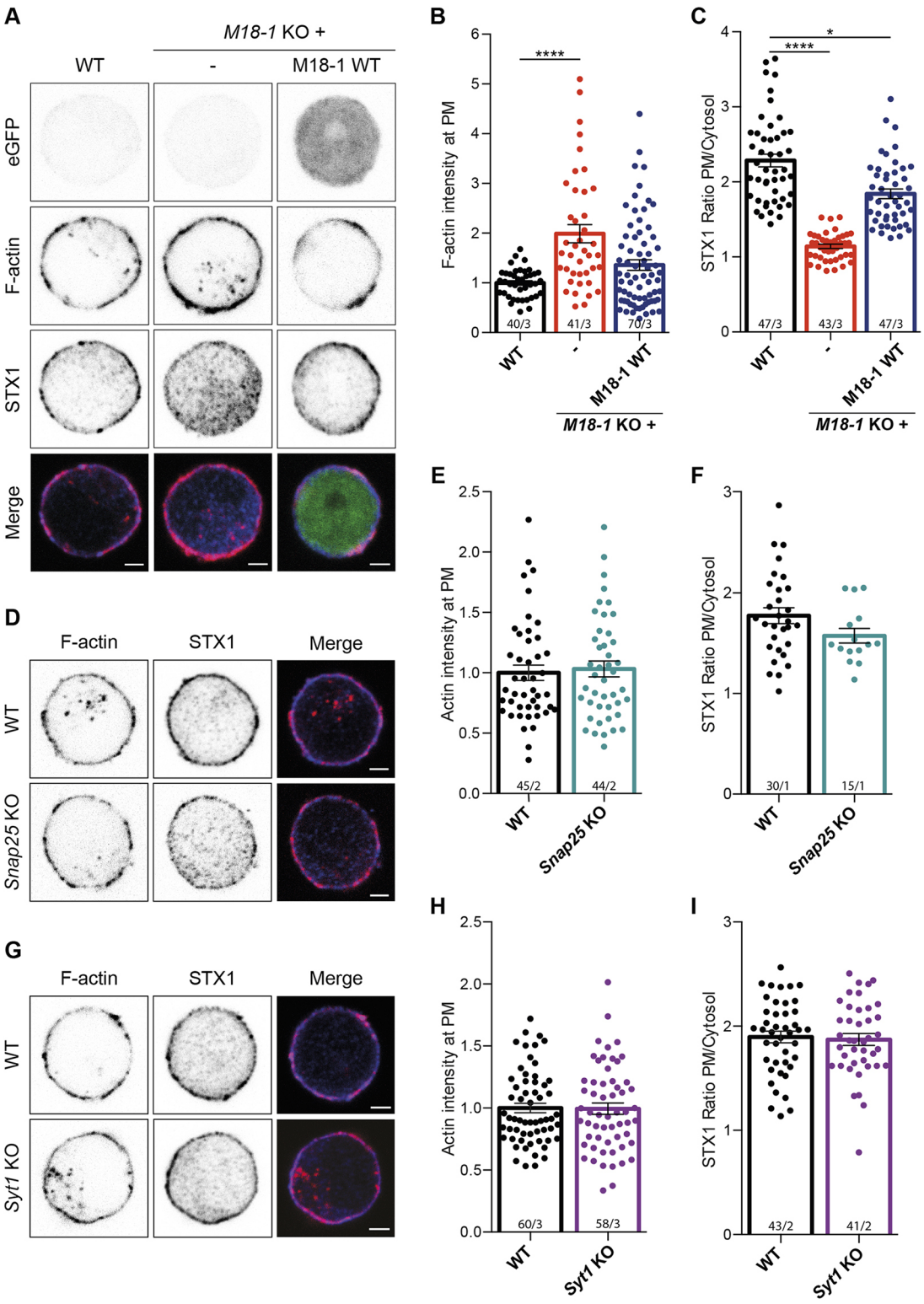

Fig. 1. Increased F-actin network levels and STX1 mistargeting are phenotypes specific for *Munc18-1*-KO MCCs. (A) Confocal images of MUNC18-1 (M18-1) WT, *Munc18-1*-KO or *Munc18-1*-KO cells expressing MUNC18-1 WT MCCs labeled with Rhodamine–phalloidin to visualize cortical F-actin. Top row, eGFP signal reporting lentivirus expression; second row, Rhodamine–phalloidin labeling F-actin; third row, STX1 labeling; bottom row, merge of three signals. (B) Quantification of F-actin intensity at the PM normalized to the levels of MUNC18-1 WT (set at 1). (C) Quantification of STX1 signal ratio (PM intensity:cytosol intensity) in MUNC18-1 WT, *Munc18-1*-KO cells and *Munc18-1*-KO cells expressing MUNC18-1 WT. (D,G) Confocal images of WT MCCs and *Snap25*-KO MCCs (D) or *Syt1*-KO MCCs (G) labeled with Rhodamine–phalloidin staining F-actin (first column) and STX1 staining (second column). The third column shows the merge of both signals. (E,H) Quantification of F-actin intensity at the PM normalized to the levels of the respective WT cells. (F,I) Quantification of the ratio STX1 signal at the PM to that in the cytosol (PM intensity:cytosol intensity) in WT cells and *Snap25*-KO or *Syt1*-KO MCCs, respectively. Bars show mean±s.e.m. *n* and *N* numbers (overall cell numbers and embryo numbers, respectively; given as *n*/*N*) are shown in each graph. **P*<0.05, *****P*<0.0001. Scale bars: 2 µm.

Journal of Cell Science (2019) 132, jcs234674. doi:10.1242/jcs.234674

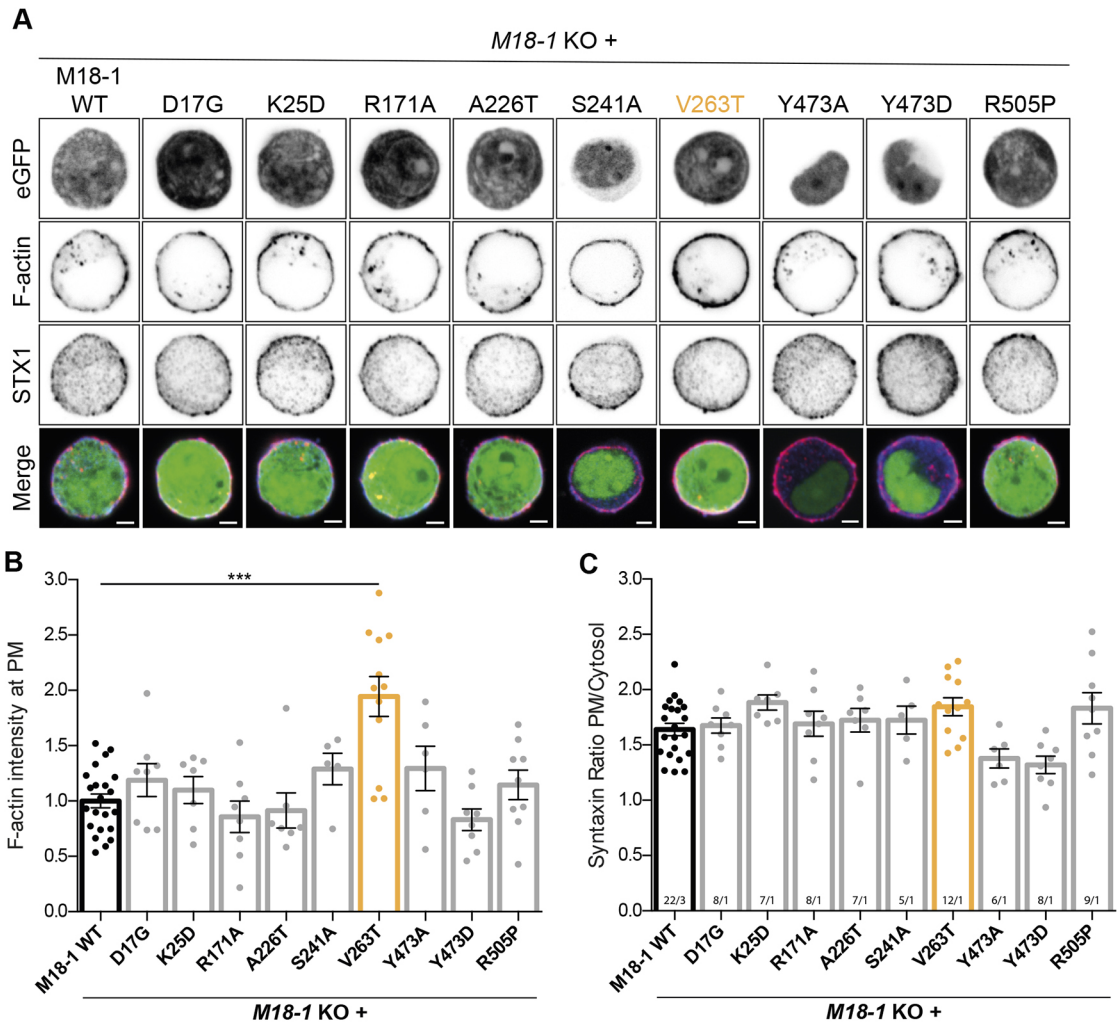

Fig. 2. Screening of F-actin and STX1 phenotypes in MUNC18-1 mutants. (A) Confocal images of *Munc18 1*-KO (*M18-1* KO) MCCs, expressing WT MUNC18-1 or the different MUNC18-1 mutant variants D17G, K25D, R171A, A226T, S241A, V263T, Y473A, Y473D, R505P (details are in Table S1). Top row, eGFP signal indicating lentivirus expression; second row, Rhodamine–phalloidin signal used to visualize F-actin; third row, STX1 staining; bottom row, merge of all three channels. (B) Quantification of cortical F-actin intensity at the plasma membrane normalized to value in *Munc18-1*-KO MCCs expressing MUNC18-1 WT (set at 1). (C) Ratio of STX1 signal at the PM to that in the cytosol (PM intensity:cytosol intensity). Bars show mean±s.e.m. *n* and *N* numbers (given as *n*/*N*) are shown in C. ***P<0.001. Scale bars: 2 µm.

and mouse (m)Vps45 appear to regulate F-actin in the same way as MUNC18-1 WT. We expanded this data set by expressing *C. elegans* Unc18, and mVps33a and mVps45 in *Munc18-1*-KO cells; these homologs all contain a hydrophobic residue at position 263 (Fig. 4A). Typical examples of the different conditions tested are shown in Fig. 4C. The expression of Unc18 in *Munc18-1*-KO cells resulted in a reduction of F-actin intensity (0.76±0.08, 24% reduction), comparable to what was seen with WT MUNC18-1 (1.0±0.07). The expression of mVps33a or mVps45 also showed similar F-actin intensity to cells expressing MUNC18-WT (Vps33a, 1.22±0.14; Vps45, 1.08±0.16) (Fig. 4D).

A hydrophobic residue in β-sheet 10 is necessary and sufficient to prevent F-actin network accumulation

Several SM proteins have a hydrophobic residue at the equivalent position of MUNC18-1(V263), but not MUNC18-2 and -3, two SM-proteins that do not support synchronous synaptic vesicle release (He et al., 2017; Santos et al., 2017) (Fig. 4A). The fact that MUNC18-2 and 3 do not have a hydrophobic residue at the position equivalent to 263 in MUNC18-1, suggests that these two paralogs may not support a normal F-actin network. We tested this, and STX1 targeting, in *Munc18-1*-KO MCCs (Fig. 5A–C). In Fig. 5A, examples of the different conditions tested are shown. Indeed, *Munc18-1*-KO MCCs expressing MUNC18-2 and -3 show an abnormally dense cortical F-actin network [MUNC18-2=1.39±0.07; MUNC18-3=1.57±0.12; similar to what is found in the MUNC18-1-KO, of 1.67±0.09, and MUNC18-1-KO with MUNC18-1(V263T), of 1.78±0.13; Fig. 5B]. All MUNC18 paralogs expressed in *Munc18-1*-KO cells restored STX1 targeting [*Munc18-1*-KO=0.99±0.02; MUNC18-1=1.42±0.05; MUNC18-2=1.33±0,04; MUNC18-3=1.26±0.03; MUNC18-1(V263T)=1.57±0,05; Fig. 5C]. To test whether this hydrophobic residue was sufficient to regulate F-actin network, we expressed MUNC18-2(T263V) and MUNC18-3(T268V) in *Munc18-1*-KO cells (Fig. 5D–F). In Fig. 5D, typical examples of the conditions studied are shown. Again, a normal F-actin network was not restored by expressing MUNC18-1 paralogs (MUNC18-2=1.84±0.1; MUNC18-3=1.82±0.13; KO=2.14±0.09; Fig. 5E). However, MUNC18-2(T263V) and MUNC18-3(T268V) did, to similar levels to what was seen with MUNC18-1 WT [MUNC18-2(T263V)=1.1±0.07; MUNC18-3(T268V)=1.06±0.06;

Journal of Cell Science (2019) 132, jcs234674. doi:10.1242/jcs.234674

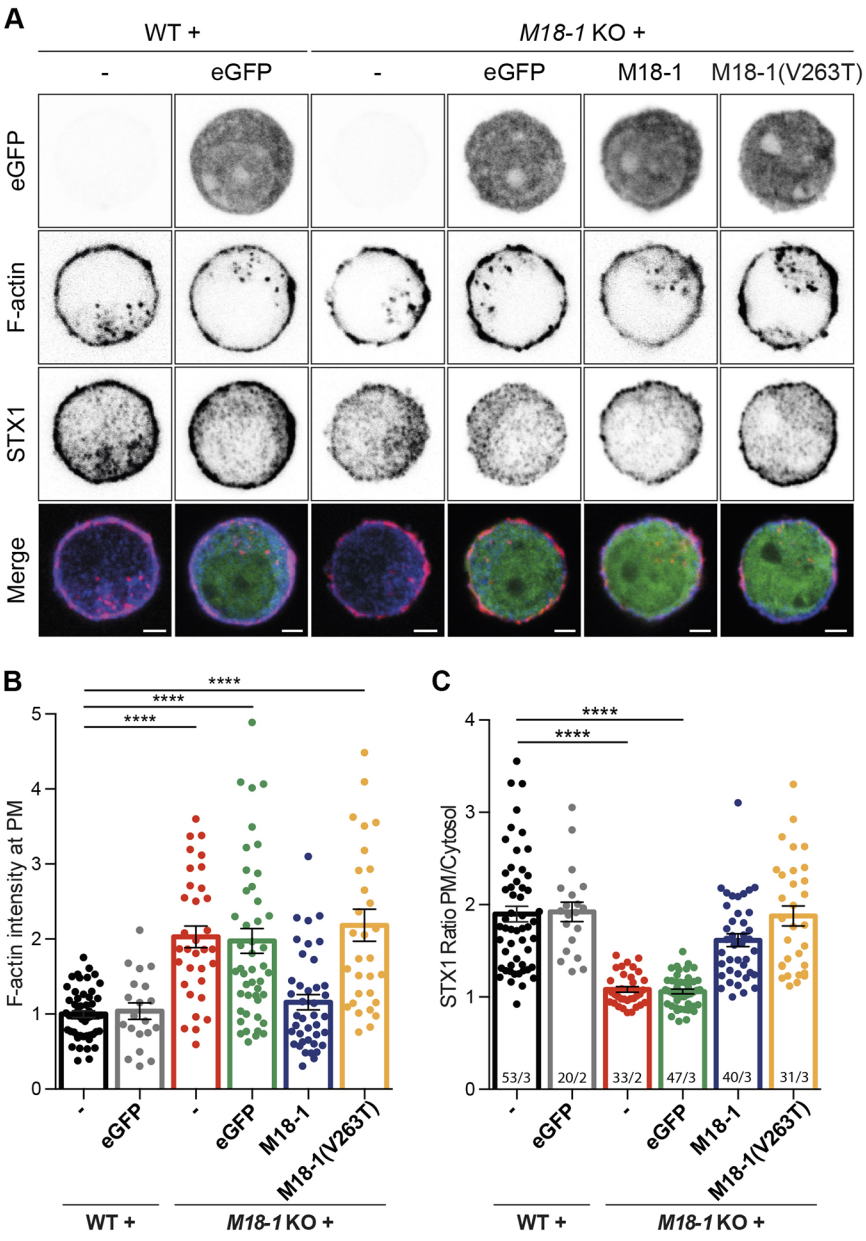

Fig. 3. MUNC18-1(V263T) regulates STX1 targeting but not F-actin network intensity in *Munc18-1*-KO MCCs. (A) Confocal images of MUNC18-1 (M18-1) WT MCCs and *Munc18-1*-KO MCCs expressing or not expressing eGFP, and *Munc18-1*-KO MCCs expressing MUNC18-1 WT or the mutant MUNC18-1(V263T). First row, eGFP signal reporting lentivirus (IRES) expression; second row, Rhodamine–phalloidin staining to visualize F-actin; third row, STX1 antibody staining; fourth row, merge of all three channels. (B) Quantification of cortical F-actin intensity at the PM normalized to that in MUNC18-1 WT cells (set at 1). (C) Ratio of STX1 signal at the PM to that in the cytosol (PM intensity:cytosol intensity). Bars show mean±s.e.m. *n* and *N* numbers (given as *n*/*N*) are shown in C. ****P<0.0001. Scale bars: 2 µm.

MUNC18-1 WT=1±0.06; Fig. 5E]. As shown above, MUNC18-1, -2 and -3 restored STX1 targeting. In addition, MUNC18-2 and -3 mutants also showed normal STX1 targeting [*Munc18-1*-KO= 0.99±0.02; MUNC18-1 WT=1.34±0,03; MUNC18-2=1.22± 0.03; MUNC18-2(T263V)=1.25±0.03; MUNC18-3=1.25±0.04; MUNC18-3(T268V)=1,29±0.04; Fig. 5F].

The observation that MUNC18-3 restored STX1 targeting in *Munc18-1*-KO cells is unexpected as this paralog was previously reported to interact with other STX paralogs (predominantly STX2 and STX4) (Tamori et al., 1998; Tellam et al., 1997). We tested the interaction between MUNC18-1 or -3 with STX1 using co-immunoprecipitation from HEK293 cell lysate. Precipitation of MUNC18-1 or -3 robustly co-precipitated STX1 (Fig. 5G). Hence, all MUNC18 paralogs bind and target STX1.

A summary of the SM proteins studied in this manuscript, the percentage of similarity to MUNC18-1, and their role in regulating F-actin are shown in Table S2. These data show that a hydrophobic residue in the position equivalent to V263 in MUNC18-1 is necessary and sufficient to regulate the F-actin network.

MUNC18-1(V263T) supports normal secretory vesicle docking

By using the MUNC18-1(V263T) mutant, we assessed whether the increased cortical F-actin levels are sufficient to explain the docking defect previously observed in *Munc18-1*-KO cells (Toonen et al., 2006; Voets et al., 2001) by chemical fixation and electron microscopy. Typical examples of the cells and the conditions tested are shown in Fig. 6A. The docking defect in *Munc18-1-KO* MCCs compared to WT (78% reduction, Fig. 6A–D) was confirmed. This defect was similar when eGFP was expressed as a negative control (70% reduction). The expression of MUNC18-1 WT restored docking in *Munc18-1*-KO cells to WT levels (WT cells, 15.60±1.86 docked vesicles per cross section; expression of MUNC18-1 WT in KO cells, 15.52±2.71 docked vesicles; Fig. 6C). Moreover, *Munc18-1*-KO cells expressing the MUNC18-1(V63T) mutant

Journal of Cell Science (2019) 132, jcs234674. doi:10.1242/jcs.234674

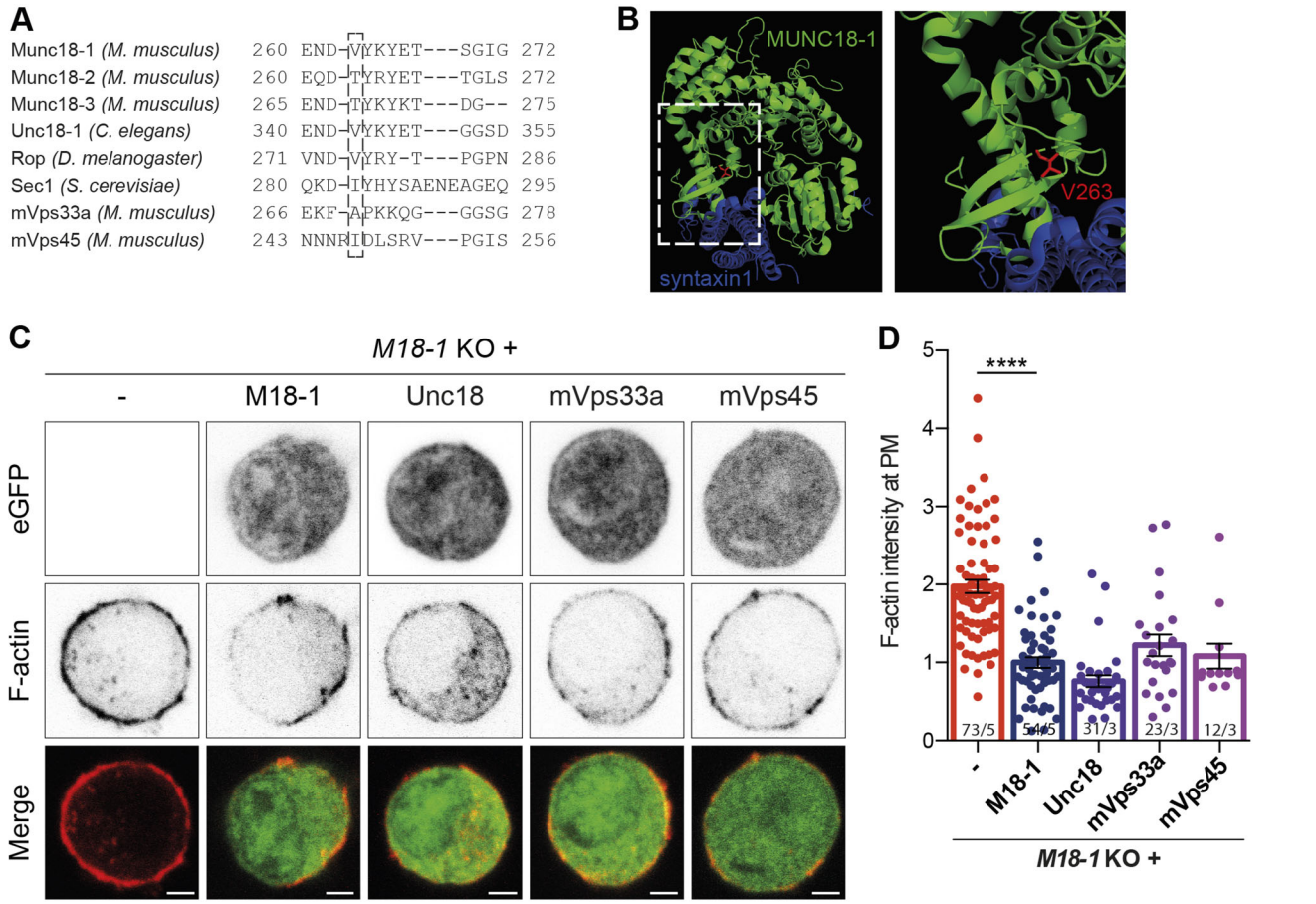

Fig. 4. F-actin intensity regulation is a feature of several SM proteins. (A) Alignment of the amino acid sequence surrounding V263 residue of mouse MUNC18-1, MUNC18-2, MUNC18-3, mVps33a and mVps45; *C. elegans* UNC18; *D. melanogaster* Rop and yeast Sec1. (B) Crystal structure of the MUNC18-1 (green) bound to closed STX1 (blue) showing where is the V263 residue (red), adapted from Burkhardt et al. (2008) (PDB code 3C98). A magnification showing the 10th and 11th β-sheet and the localization of the V263 residue is shown on the right. (C) *Munc18-1-KO* MCCs (*M18-1* KO), either expressing or not expressing different SM proteins (MUNC18-1, Unc18, mVps33a and mVps45). Top row, eGFP, reporting SFV expression; middle row, Rhodamine–phalloidin labeling; bottom row, merge of both signals. (D) Quantification of cortical F-actin intensity at the plasma membrane normalized to that in *Munc18-1*-KO MCCs expressing MUNC18-1 WT (set at 1). Bars show mean±s.e.m. *n* and *N* numbers (given as *n*/*N*) are shown. ****P<0.0001. Scale bars: 2 µm.

showed a similar number of docked vesicles (11.15±1.35) to WT cells or *Munc18-1*-KO cells expressing MUNC18-1 WT (Fig. 6B). The expression of the eGFP, MUNC18-1 or MUNC18-1(V263T) did not affect the total number of vesicles with an average of ∼120 vesicles per section (range from 107.5±10.71 to 131.7±9.79, Fig. 6C). The distribution of the vesicles relative to the PM when expressing MUNC18-1(V263T) is similar to that in WT cells (Fig. 6D). These results show that MUNC18-1(V263T) restores docked vesicles to a normal level without restoring the cortical F-actin network in *Munc18-1*-KO cells. This indicates that the extensive cortical F-actin network in *Munc18-1*-KO cells is not a rate limiting barrier for secretory vesicle docking.

MUNC18-1(V263T) supports normal regulated secretion

We next tested whether the restored docked pool of secretory vesicles by MUNC18-1(V263T) expression also supported regulated secretion using Ca^{2+} uncaging and membrane capacitance measurements. Uncaging Ca^{2+} in MUNC18-1 WT cells evoked a robust secretion response (black trace, Fig. 7A) with many vesicles fusing in the first few hundred milliseconds after uncaging (burst) and a subsequent linear phase (sustained release). In line with previous reports, *Munc18-1*-KO cells showed strongly impaired secretion (red trace, Fig. 7A) (Toonen et al., 2006; Voets et al., 2001). Expression of MUNC18-WT and MUNC18-1(V263T) both restored the secretion response to similar levels and with similar kinetics to that seen in the WT (blue and yellow traces, respectively, Fig. 7A). The basal Ca^{2+} concentration (before the UV flash) was similar in all groups (Fig. 7B). The burst size (i.e. capacitance change in the first second after stimulation) is a measure of the secretion of primed vesicles pools [readily releasable pool (RRP) and slowly releasable pool (SRP)], which was similar in MUNC18-1 WT cells and *Munc18-1*-KO cells expressing MUNC18-1-WT or -V263T, and highly reduced in *Munc18-1*-KO cells (Fig. 7C). Sustained release and the rate of vesicle recruitment (sustained release rate) were also similar in MUNC18-1-WT and -V263T expressing cells (Fig. 7D,E). These data show that MUNC18-1 with the V263T mutation supports normal secretion, a normal RRP and normal vesicle recruitment during stimulation. This indicates that the increased cortical F-actin network in *Munc18-1*-KO cells is not a limiting barrier for normal regulated secretion.

DISCUSSION

This study addressed two cellular functions of MUNC18-1 in chromaffin cells, the regulation of submembrane F-actin and the targeting of STX1 to the plasma membrane. We found that the abnormal F-actin network in the absence of MUNC18-1 is not a

Journal of Cell Science (2019) 132, jcs234674. doi:10.1242/jcs.234674

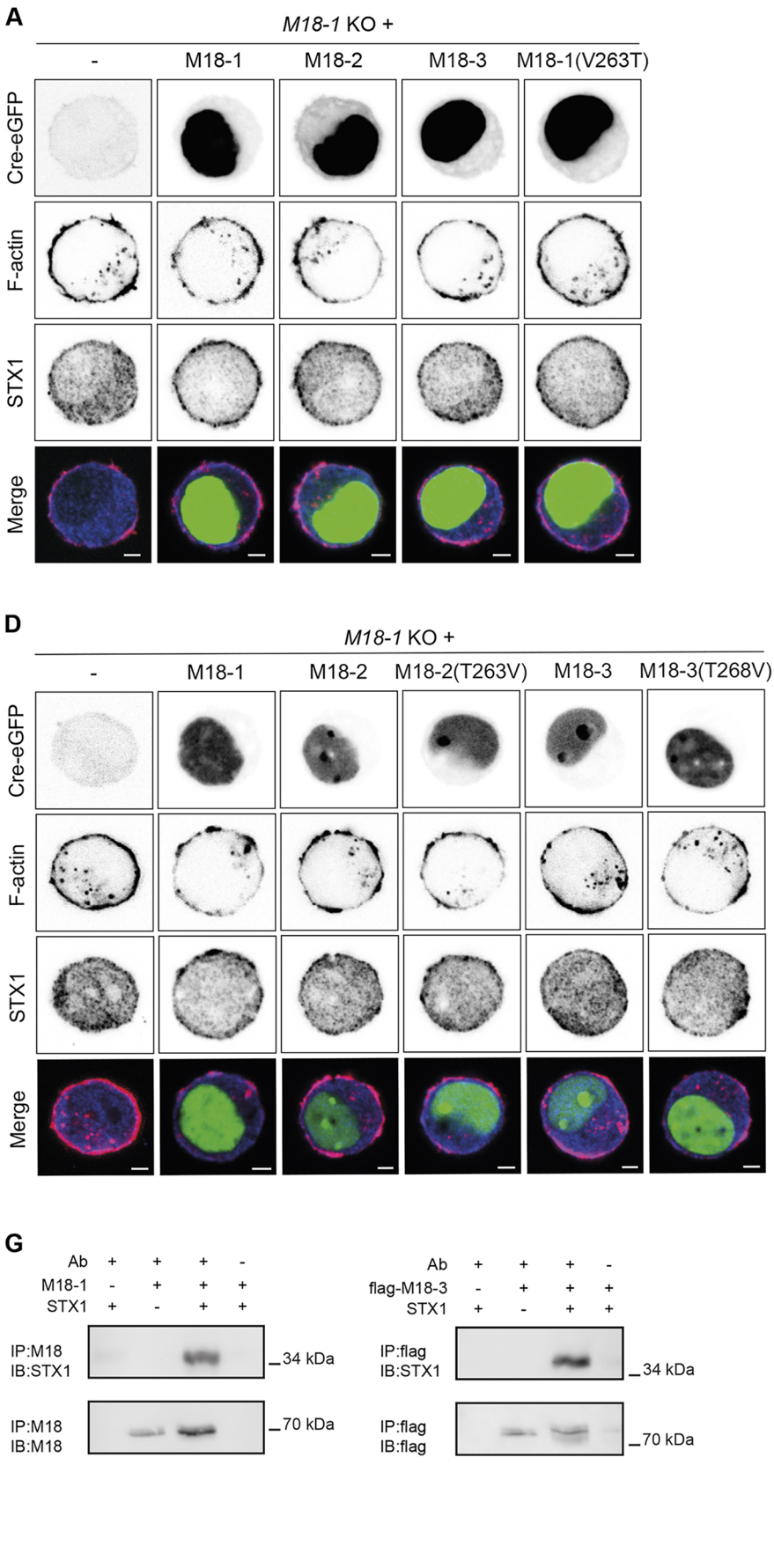

Fig. 5. See next page for legend.

Journal of Cell Science (2019) 132, jcs234674. doi:10.1242/jcs.234674

Fig. 5. The F-actin network is regulated by a hydrophobic residue at position 263 of MUNC18-1. (A) Confocal images of *Munc18-1*-KO (*M18-1* KO) MCCs either not infected or expressing MUNC18-1, MUNC18-2, MUNC18-3 or MUNC18-1(V263T). First row, nucleus-targeted Cre-eGFP signal reporting lentivirus expression; second row, Rhodamine–phalloidin staining to visualize F-actin; third row, STX1 antibody staining; fourth row, merge of all three channels. (B) Quantification of cortical F-actin intensity at the PM normalized to that in *Munc18-1*-KO MCCs expressing MUNC18-1 WT (set at 1). (C) Ratio of STX1 signal at the PM to that in the cytosol (PM intensity: cytosol intensity). (D) Confocal images of *Munc18-1*-KO MCCs either expressing or not expressing WT MUNC18-1, MUNC18-2, MUNC18-3 or the mutants MUNC18-2(T263V) and MUNC18-3(T268V). First row, nucleus-targeted Cre-eGFP signal reporting lentivirus expression; second row, Rhodamine–phalloidin staining to visualize F-actin; third row, STX1 antibody staining; fourth row, merge of all three channels. (E) Quantification of cortical F-actin intensity at the PM normalized to that in *Munc18-1*-KO MCCs expressing MUNC18-1 WT. (F) Ratio of STX1 signal at the PM to that in the cytosol (PM intensity:cytosol intensity). (G) Typical blots of co-immunoprecipitation (IP) of HEK293 cell lysates with MUNC18-1 or MUNC18-3 (M18-3) and STX1 (left, M18-1; right Flag-tagged M18-3) with the respective controls. Bars show mean±s.e.m. *n* and *N* numbers (given as *n*/*N*) are shown in C and F. ***P*<0.01, *****P*<0.0001. Scale bars: 2 µm.

general consequence of docking and secretion defects, because such accumulation was not observed in *Snap25*- and *Syt1*-KO cells. We identified a point mutation, MUNC18-1(V263T), which restored STX1 targeting, but not a normal F-actin network. We conclude that MUNC18-1 regulates the F-actin network and STX1 targeting by distinct mechanisms. Moreover, MUNC18-1(V263T) fully restored vesicle recruitment, docking and fusion in KO cells, indicating that the increased F-actin network in these cells is not a rate-limiting barrier for secretory vesicle trafficking and fusion.

A hydrophobic residue at position 263 in SM proteins is necessary and sufficient for F-actin regulation

The MUNC18-1(V263T) mutant provides separation of the F-actin-regulating role of MUNC18-1 and its other roles in STX1 targeting, docking and secretion. This mutant was designed based on a homology mismatch in β-sheet 10 of MUNC18-1 versus MUNC18-2 and MUNC18-3. While the sequence NDVY is conserved in orthologs Rop1 (*D. melanogaster*) and Unc18 (*C. elegans*), MUNC18-2 and -3 have a threonine (DTY, like the mutant V263T). Hence, a hydrophobic amino acid is present in homologs that regulate actin and a polar amino acid is in the ones that do not. Consistent with this, the MUNC18-1(V263T) lost the ability to regulate F-actin while MUNC18-2(T263V) and MUNC18-3(T368V) mutants gained this ability. The sequence around residue V263 of MUNC18-1, at the start of β-sheet 10, may be an effector domain for SM proteins that regulate F-actin. The sequence at this specific site explains why some relatively distant homologs of MUNC18-1, with overall less

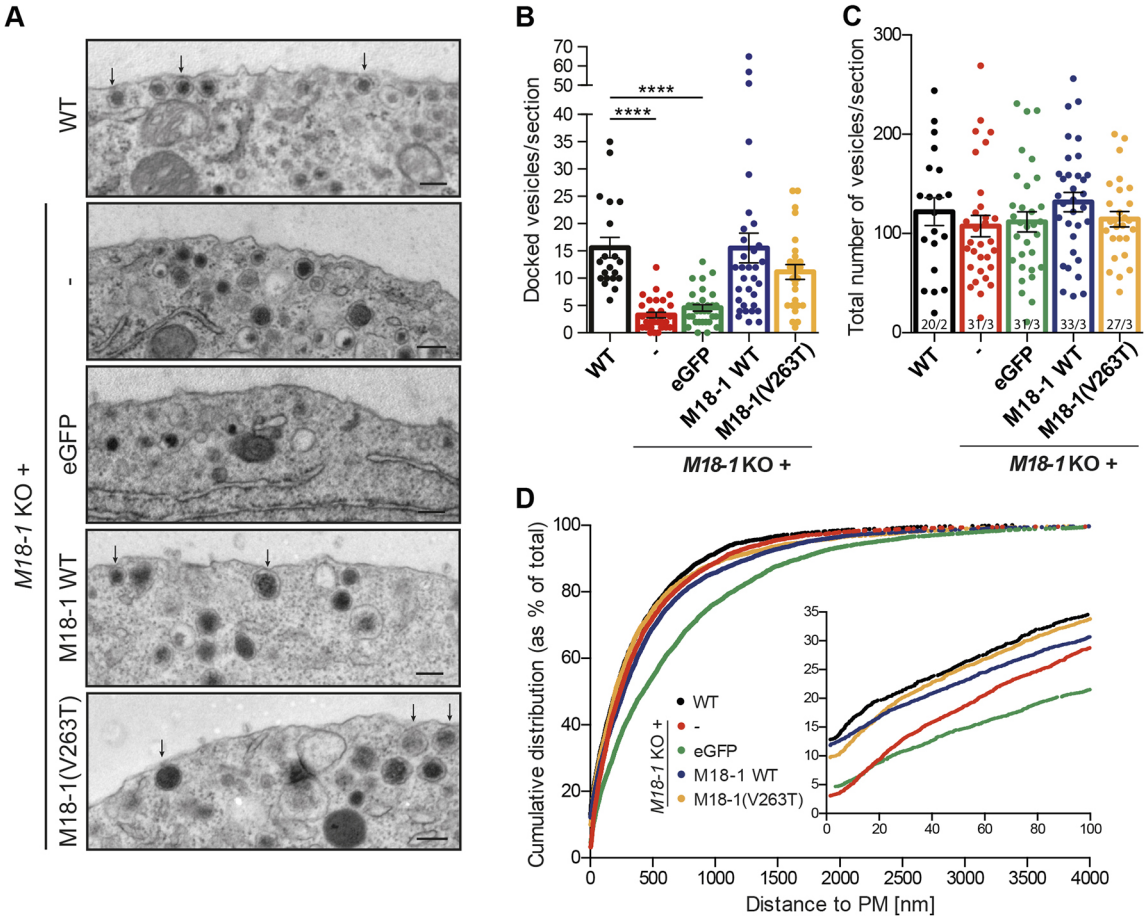

Fig. 6. MUNC18-1(V263T) restores vesicle docking in *Munc18-1*-KO MCCs. (A) Typical ultrastructural images of the PM area of WT MCCs and *Munc18-1*-KO (*M18-1* KO) cells infected or not infected with eGFP (negative control), MUNC18-1 WT or MUNC18-1(V263T), as indicated. Arrows indicate docked vesicles. Scale bars: 200 nm. (B) Number of docked vesicles per cross section. (C) Total number of vesicles per cross section. (D) Normalized cumulative distribution of vesicles as a function of the distance from the plasma membrane. Insert, magnification of the area at 0–100 nm from the PM. Bars show mean±s.e.m. *n* and *N* numbers (given as *n*/*N*) are shown in B. *****P*<0.0001.

Journal of Cell Science (2019) 132, jcs234674. doi:10.1242/jcs.234674

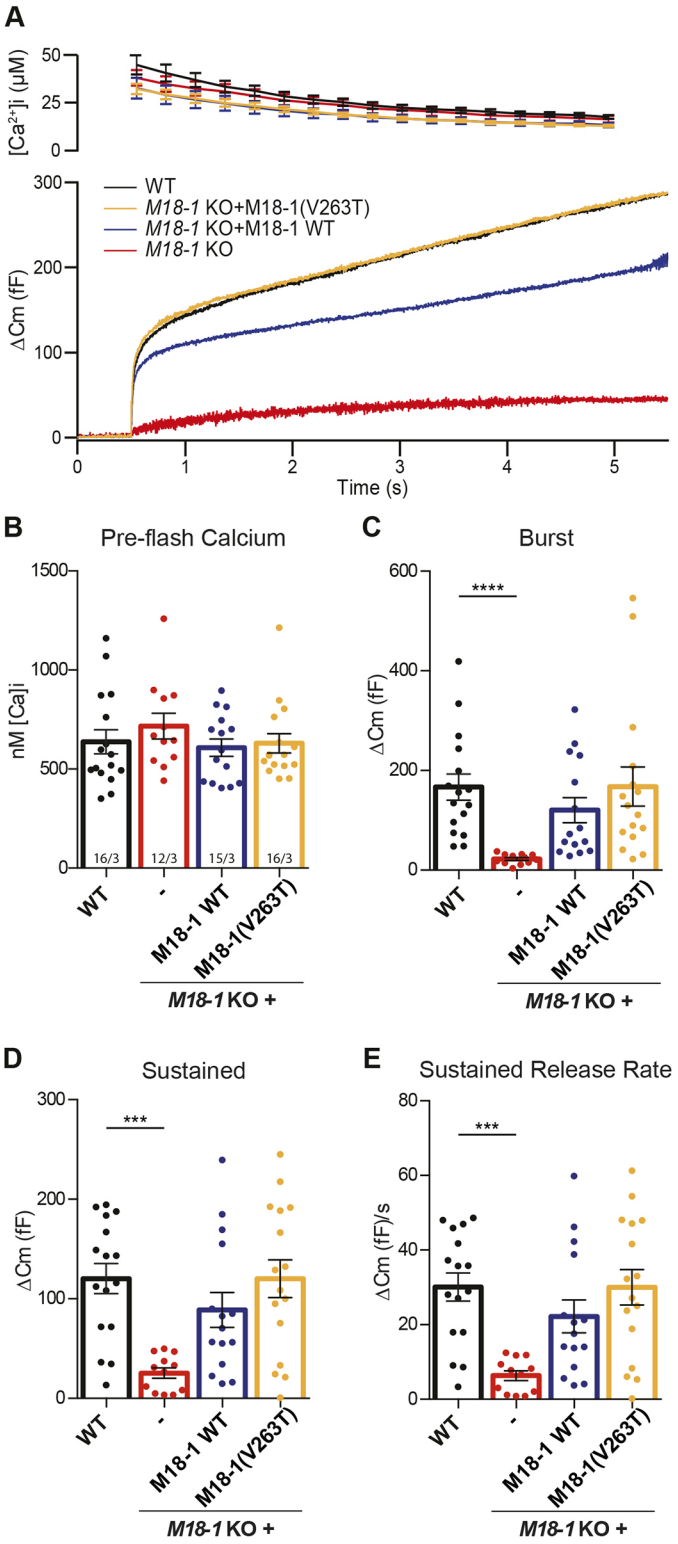

Fig. 7. MUNC18-1(V263T) mutant rescues secretion in *Munc18-1*-KO MCCs. (A) Ca^{2+}-uncaging experiment showing means for all measured cells. Top, mean±s.e.m. $[Ca^{2+}]_i$ following the flash. Bottom, mean capacitance measurements. Measurements are of MUNC18-1 WT (black), *Munc18-1*-KO (red), and *Munc18-1*-KO cells expressing MUNC18-1 (blue) or MUNC18-1(V263T) (yellow). (B) Quantification of pre-flash $[Ca^{2+}]_i$. (C–E) Quantification of (C) burst size, (D) sustained release and (E) sustained release rate in MUNC18-1 WT MCCs and *Munc18-1*-KO either not transfected or expressing MUNC18-1 WT or V263T. Bars show mean±s.e.m. *n* and *N* numbers (given as *n*/*N*) are shown in B. ***P<0.001, ****P<0.0001.

similarity to MUNC18-1, still regulate F-actin while more similar paralogs do not.

A hydrophobic residue at position 263 is dispensable for STX1 targeting, docking and fusion

Expression of MUNC18-1(V263T), MUNC18-2 and -3 all restored STX1 targeting to the PM similar to MUNC18-1-WT. MUNC18-1 and -2 are known to bind STX1 with high affinity, but MUNC18-3 was shown to interact only weakly with STX1 compared to its strong binding to STX2 and STX4 (Tamori et al., 1998; Tellam et al., 1997). However, we show that MUNC18-3 robustly interacts with STX1 (Fig. 5G), when it is abundantly expressed. Apparently, this interaction is sufficient to target STX1 correctly, similar to MUNC18-1 (Gulyas-Kovacs et al., 2007).

Domain 3a is the central domain in MUNC18-1 responsible for SNARE complex assembly (so-called ‘SNARE templating’; Baker et al., 2015) and making vesicles fusion competent (Han et al., 2014; Jiao et al., 2018; Munch et al., 2016; Parisotto et al., 2014). Previously described mutations or deletions in this domain that interfere with SNARE templating generally do not affect STX1 targeting to the membrane (Martin et al., 2013; Munch et al., 2016, but see Han et al., 2014). In line with these findings, the V263T mutation also supports normal STX1 targeting. Furthermore, the V263T mutation also supports normal vesicle recruitment, priming and fusion, suggesting that the part of domain 3a surrounding β-sheet 10 is not directly involved in SNARE templating. Hence, because other aspects of MUNC18-1 function remain unaffected by the substantial change at this side of domain 3a (a valine residue to a threonine residue), it seems likely that this side is specifically involved in F-actin regulation.

Hence, the V263T mutant provides separation between F-actin regulation and STX1 targeting functions of MUNC18-1. This separation seems a rare event given that all other mutants tested here as well as several orthologs support both functions. The exact pathway for F-actin regulation remains unknown. The hydrophobic residue may be involved in a lipid interaction. For instance, phosphoinositides are well known to regulate F-actin (for a review, see Saarikangas et al., 2010).

An increased submembrane F-actin network does not impair normal docking and secretion

It has been proposed that there could be both positive and negative roles for submembrane F-actin in secretory vesicle exocytosis; namely, that it might have a transport (facilitative) or a ‘barrier’ role (Meunier and Gutiérrez, 2016; Porat-Shliom et al., 2013). The F-actin network is reorganized and remodeled upon stimulation (Vitale et al., 1995, 1991) and activation of the diacylglycerol signaling pathway (DAG) (Vitale et al., 1995). As a consequence, the number of vesicles in close proximity to the PM (Gil et al., 2000; Giner, 2005; Papadopulos et al., 2015) and the initial release rate are increased (Vitale et al., 1995). Hence, the reorganization of the cortical F-actin coincides with increased docking and fusion of secretory vesicles, which could be interpreted as cortical F-actin having a barrier function. Conversely, F-actin blockers slowed down release (Wen et al., 2016). Our laboratory has previously shown that morphological docking is restored in unstimulated *Munc18-1*-KO cells upon inhibition of actin polymerization by latrunculin A, but these docked vesicles are unable to fuse upon stimulation (Toonen et al., 2006). Our current results argue against a barrier function: expressing MUNC18-1(V263T) restored both docking and secretion in *Munc18-1-KO* MCCs even though the cells had an F-actin network that was twice as dense (Figs 6 and 7). This indicates that the increased F-actin network in absence of

MUNC18-1 does not limit the RRP and also does not affect vesicle recruitment to the releasable pool during stimulation (Fig. 7).

While secretion does not require MUNC18-1-dependent F-actin regulation, our data do not exclude that other aspects of submembrane F-actin reorganization are still important for regulated secretion in MCCs. Ca^{2+} uncaging as used in this study, may still reorganize the F-actin network, as shown upon nicotine, high K^+ or phorbol ester stimulation (Vitale et al., 1995), in a MUNC18-1-independent manner. This may explain why F-actin blockers slowed down release in chromaffin cells (Wen et al., 2016).

In conclusion, we have uncovered a conserved region in SM proteins that regulates F-actin network independently of their canonical role of STX1 targeting and membrane fusion. Our experiments show that an abnormally dense cortical F-actin network cannot explain the docking, priming and fusion deficits observed in *Munc18-1*-KO cells, indicating that dense cortical F-actin does not function as a rate-limiting barrier for secretory vesicles docking and fusion in MCCs.

MATERIALS AND METHODS

Laboratory animals

Munc18-1, *Snap25* and *Syt1*-KO mice generation was described earlier (Verhage et al., 2000; Washbourne et al., 2002; Geppert et al., 1994). Heterozygote mice of MUNC18-1, SNAP25 and SYT1 were timely bred to obtain embryos [embryonic day (E)18] through caesarean section of the pregnant females. Laboratory animals were housed and bred according to institutional and Dutch or Danish governmental guidelines for animal welfare.

Primary cell culture and transfection

Mouse chromaffin cells (MCCs) from embryonic (E18) wild-type, *Munc18-1*-KO, *Snap25*-KO and *Syt1*-KO mice were isolated as described previously (Sørensen et al., 2003). The isolated cells were cultured on rat tail collagen-coated 18 mm glass coverslips. MCCs were maintained at 37°C and 10% CO_2 for 3 days. When necessary, cells were infected on day *in vitro* (DIV) 0 for 3 days at 37°C with Lentivirus containing full-length *M18-1-IRES-eGFP* (Figs 1, 2, 3 and 7), *M18-1(V263T)-IRES-eGFP* (Figs 2, 3 and 7) and *IRES-eGPF* as a control (Fig. 3). In Fig. 2, *M18(D17G)-IRES-eGFP*, *M18(K25D)-IRES-eGFP*, *M18(R171A)-IRES-eGFP*, *M18(A226T)-IRES-eGFP*, *CreEGFP-T2a-M18(S241A)*, *CreEGFP-T2a-M18(Y473A)*, *CreEGFP-T2a-M18(Y473D)* and *M18(R505P)-IRES-eGFP* were used. In addition, T2a constructs were used to express MUNC18-1 [*iCre-EGFP-T2A-m18-1(WT)*], MUNC18-2 (*iCre-EGFP-T2A-m18-2*), MUNC18-3 [*iCre-EGFP-T2A-m18-3*] and the mutants MUNC18-1(V263T) [*iCre-EGFP-T2A-m18(V263T)*], MUNC18-2(T263V) [*iCre-EGFP-T2A-m18-2(T263V)*] and MUNC18-3(T268V) [*iCre-EGFP-T2A-m18-3(T268V)*] for Fig. 5. Otherwise, cells were infected on DIV3 for 8–12 h with Semliki Forest Virus (SFV), previously activated by chymotrypsin and aprotinin. SFV containing *Munc18-1-IRES-eGFP*, *Munc18-1(V263T)-IRES-eGFP*, IRES-eGFP were used for docking experiments (Fig. 6) and *unc18-IRES-eGFP*, *Vps33a-IRES-eGFP*, *Vps45-IRES-eGFP* for assessing F-actin intensity (Fig. 4).

Immunocytochemistry and confocal imaging

MCCs were fixed with 4% paraformaldehyde (Merck) in phosphate-buffered saline (PBS), pH 7.4, for 1 h at room temperature. The cells were permeabilized for 5 min with PBS containing 0.5% Triton X-100 (Thermo Fisher Scientific). Cells were blocked with PBS containing 2% normal goat serum (Life Technologies) and 0.1% Triton X-100 for 30 min at room temperature. All antibodies were diluted in this solution, and incubation with primary and secondary antibodies was undertaken at room temperature for 2 h or 1 h, respectively. Specific primary antibodies used were against: syntaxin1 (rabbit polyclonal, 1:1000, I379 a gift from the Südhof laboratory, Department of Molecular and Cellular Physiology, Stanford University School of Medicine, USA) and MUNC18-1 (rabbit polyclonal, 1:1000, SySy, Cat. No. 116002). The F-actin network was stained with the conjugate Rhodamine–phalloidin (R415, Molecular Probes, 1:1000), which does not require a secondary antibody. Alexa-Fluor-conjugated secondary antibodies were purchased from Invitrogen. Coverslips were mounted on glass microscopy slides using Dabco-Mowiol (Sigma). To image the stained cells, a confocal laser scanning microscope (LSM 500 meta; Carl Zeiss Microimaging) was used. Images were taken using a 63×1.4 numerical aperture oil-immersion objective lens. An additional zoom factor of 5 was applied and the images were acquired with a frame size of 1024×1024 pixels. The analysis of the images was primarily executed with PlasMACC, which is implemented as a plugin in the image analysis software Fiji (Kurps et al., 2014). The intensity of fluorescent signals was determined at the PM. In order to calculate the ratio between the signal intensity at the PM and the cytosol, pixel intensities were measured inside of the region of interest (ROI). The mean of the intensity signal at the PM was divided by the mean intensity in the cytosol.

Co-immunoprecipitation and western blotting

HEK293T cells (ATCC) were seeded to 60% confluency on the day of transfection. HEK cells were transfected with MUNC18-1 [iCre-EGFP-T2A-*M18-1(WT)*], Flag–MUNC18-3 (*FlagTag-Munc18-3*) or syntaxin1 (*STX1-IRES-eGFP*). Cells were lysed in IP-buffer [50 mM Tris-HCl pH 7.5, 1% Triton X-100, 1.5 mM $MgCl_2$, 5.0 mM EDTA, 100 mM NaCl, and protease Inhibitor cocktail (Sigmafast)] at 24 h after transfection. Cells were centrifuged at 20,000 ***g*** for 10 min 4°C and the supernatants were combined. Antibody against MUNC18-1 (mouse monoclonal, 1:1000, 610336 BD Transduction Laboratories) or Flag (mouse monoclonal, 1:1000, F1804, Sigma-Aldrich) was added and the samples were tumbled 16 h at 4°C. After this, Protein A–agarose beads (vector shield) were added and rotated for 1 h at 4°C. Then, the immunoprecipitations were washed five times with IP-buffer and the samples were eluted from the beads with Laemmli sample buffer. The IP samples were run on a SDS-PAGE and transferred to a PVDF membrane (Bio-Rad). The membrane was blocked with 2% milk plus 0.5% BSA (Merck) in PBS with 0.1% Tween-20 (PBS-T) for 45 min. Next, the membranes were incubated with antibodies against syntaxin1 (HPC-1, Sigma 1:1000), MUNC18-1 (1:1000) or Flag (1:1000) overnight at 4°C. Then, membranes were incubated with secondary alkaline phosphatase-conjugated antibodies (1:10,000, Jackson ImmunoResearch) for 30 min at room temperature. AttoPhos (Promega) was used for visualization and membranes were scanned with a FLA-5000 fluorescent image analyser (Fujifilm).

Electron microscopy

MCCs were fixed at DIV3 using a conventional chemical fixation protocol with 2.5% glutaraldehyde (Merk) in 0.1 M cacodylate buffer, pH 7.4, overnight at 4°C. Cells were washed with 0.1 M cacodylate buffer and post fixed with 1%OsO_4/1%$Ru(CN)_6$ for 45 min at room temperature. A series of increasing ethanol concentrations (30–100%) were used to dehydrate the samples, followed by embedding in EPON (24 g glycin ether, 16 g DDSA, 10 g MNA, 1.3 ml BDMA) and polymerization for 48 h at 65°C. The coverslip was removed from EPON resin by alternatively dipping it into liquid nitrogen and boiling water. High-cell density monolayers were selected, cut and mounted on prepolymerized EPON blocks for thin sectioning. Ultrathin sections of 70 nm were cut parallel to the cell monolayer, collected on single-slot formvar coated copper grids, and stained with uranyl acetate (Ultrostain I, laurylab) and lead citrate (Reynolds) in a Leica EM AC20 Ultra stainer. For high resolution imaging, a Jeol 1010 transmission electron microscope was used. For each condition, the total number of vesicles, the number of docked vesicles and the distance to the PM were measured using the measuring tool of FIJI software or a custom-written semiautomatic image analysis software running in Matlab (MathWorks) (available upon request). We considered vesicles as docked when no distance was visible between the vesicle membrane and the plasma membrane. Infected cells were identified based on presence of SFV (droplet shape with dense core) on the PM.

Electrophysiological recordings

Exocytosis in chromaffin cells from E18 WT or *Mun18-1*-KO littermates was measured on an Axiovert 10 inverted microscope (Carl Zeiss) mounted with Fluar 40×1.30 NA oil objective. Cells transfected with lentiviruses were incubated for 48 h prior to measurements. The transfected cells were identified by the green fluorescent response to 488 nm illumination by a monochromator

(Polychrome IV, Till Photonics). Cell membrane capacitance was monitored in whole-cell patch-clamp configuration based on the Lindau and Neher technique (1988) using an EPC-9 amplifier and Pulse Software (version 8.53) (HEKA Elektronik) with Lock-In extension in 'sinedc' mode. Currents were filtered at 3 kHz and sampled at 12 kHz. Secretion was stimulated by UV-photolysis of the Ca^{2+} cage nitrophenyl-EGTA. A 2-ms UV-light was delivered from a UV flash lamp (JML-C2, Rapp OptoElectronics) through a 395 nm band-pass filter, transmitted by a light guide and dual condenser, and focused via the objective. The released vesicle pool was determined 0.5 s after the flash and designated as the 'burst size' while the sustained release component accounts for the residual release that follows after the burst for 4 s. The intracellular Ca^{2+} concentration was determined as described by Voets et al. (2001) using fura-4F and furaptra dye excitation, measured alternating between 350 and 380 nm at 40 Hz in a pre-calibrated setup using calibration solutions with known Ca^{2+} concentrations. Emitted fura light was detected by a photo diode (Till Photonics) in an area around the cell defined by a View Finder (Till Photonics), recorded at 3 kHz and filtered at 12 kHz. Patch pipette solution contained (in mM): 100 Cs-glutamate, 8 NaCl, 4 $CaCl_2$, 32 HEPES, 2 Mg-ATP, 0.3 NaGTP, 5 nitrophenyl-EGTA, 1 ascorbic acid, 0.4 fura-4f, and 0.4 furaptra adjusted to pH 7.2 with CsOH. The extracellular solution contained (in mM): 145 NaCl, 2.8 KCl, 2 $CaCl_2$, 1 $MgCl_2$, 10 HEPES, and 11 glucose adjusted to pH 7.2 with NaOH.

Statistics

Data are expressed as mean±s.e.m. Overall cell numbers (n) and embryo numbers (N) are annotated in the figures.

The Shapiro–Wilk normality test was used to evaluate the Gaussian distribution of the data. Bartlett's test was used to test homoscedasticity of the data. When the data was normal and homoscedastic, parametric tests were used: t-test or one-way analysis of variance, and Bonferroni as a post hoc test. Otherwise, when normality or homoscedasticity tests were not passed, Mann–Whitney or Kruskal–Wallis test (Dunn's multiple test as post hoc) were used as nonparametric tests. Significance is denoted *P<0.05, **P<0.01, ***P<0.001, ****P<0.0001.

Acknowledgements

The authors thank Joke Wortel for housing and breeding the mice and her help with MCC culture, Ingrid Saarloos for her help with co-immunoprecipitation and western blotting, Robbert Zalm for cloning and lentiviral or SFV production, and Rien Dekker for assistance in electron microscopy. Electron microscopy was performed in the VU/VUmc EM facility.

Competing interests

The authors declare no competing or financial interests.

Author contributions

Conceptualization: J.R.v.W., M.V.; Methodology: M.P.-V., J.K.; Validation: M.P.-V., J.K., B.T.; Formal analysis: M.P.-V., J.K., B.T.; Investigation: M.P.-V., J.K., B.T.; Writing - original draft: M.P.-V.; Writing - review & editing: M.P.-V., J.K., B.T., J.B.S., J.R.v.W., M.V.; Visualization: M.P.-V.; Supervision: J.B.S., J.R.v.W., M.V.; Project administration: J.R.v.W., M.V.; Funding acquisition: J.B.S., M.V.

Funding

This work is supported by a European Research Council Advanced Grant (322966) of the European Union (to M.V.). The study was also supported by the Lundbeck Foundation (Lundbeckfonden) (R221-2016-1202 and R277-2018-802), the University of Copenhagen KU2016 program of excellence and the Independent Research Fund Denmark (Danmarks Frie Forskningsfond) (8020-00228A) (to J.B.S.).

Supplementary information

Supplementary information available online at
http://jcs.biologists.org/lookup/doi/10.1242/jcs.234674.supplemental

References

Baker, R. W., Jeffrey, P. D., Zick, M., Phillips, B. P., Wickner, W. T. and Hughson, F. M. (2015). A direct role for the Sec1/Munc18-family protein Vps33 as a template for SNARE assembly. *Science* **349**, 1111-1114. doi:10.1126/science.aac7906

Burkhardt, P., Hattendorf, D. A., Weis, W. I. and Fasshauer, D. (2008). Munc18a controls SNARE assembly through its interaction with the syntaxin N-peptide. *EMBO J.* **27**, 923-933. doi:10.1038/emboj.2008.37

Cheek, T. R. and Burgoyne, R. D. (1986). Nicotine-evoked disassembly of cortical actin filaments in adrenal chromaffin cells. *FEBS Lett.* **207**, 110-114. doi:10.1016/0014-5793(86)80022-9

de Wit, H., Cornelisse, L. N., Toonen, R. F. G. and Verhage, M. (2006). Docking of secretory vesicles is syntaxin dependent. *PLoS ONE* **1**, e126. doi:10.1371/journal.pone.0000126

de Wit, H., Walter, A. M., Milosevic, I., Gulyás-Kovács, A., Riedel, D., Sørensen, J. B. and Verhage, M. (2009). Synaptotagmin-1 docks secretory vesicles to syntaxin-1/SNAP-25 acceptor complexes. *Cell* **138**, 935-946. doi:10.1016/j.cell.2009.07.027

Geppert, M., Goda, Y., Hammer, R. E., Li, C., Rosahl, T. W., Stevens, C. F. and Südhof, T. C. (1994). Synaptotagmin I: a major Ca2+ sensor for transmitter release at a central synapse. *Cell* **79**, 717-727. doi:10.1016/0092-8674(94)90556-8

Gil, A., Rueda, J., Viniegra, S. and Gutiérrez, L. M. (2000). The F-actin cytoskeleton modulates slow secretory components rather than readily releasable vesicle pools in bovine chromaffin cells. *Neuroscience* **98**, 605-614. doi:10.1016/S0306-4522(00)00132-9

Gimenez-Molina, Y., Villanueva, J., Francés, M. M., Viniegra, S. and Gutiérrez, L. M. (2018). Multiple mechanisms driving F-actin-dependent transport of organelles to and from secretory sites in bovine chromaffin cells. *Front. Cell. Neurosci.* **12**, 344. doi:10.3389/fncel.2018.00344

Giner, D. (2005). Real-time dynamics of the F-actin cytoskeleton during secretion from chromaffin cells. *J. Cell Sci.* **118**, 2871-2880. doi:10.1242/jcs.02419

González-Jamett, A. M., Momboisse, F., Guerra, M. J., Ory, S., Báez-Matus, X., Barraza, N., Calco, V., Houy, S., Couve, E., Neely, A. et al. (2013). Dynamin-2 regulates fusion pore expansion and quantal release through a mechanism that involves actin dynamics in neuroendocrine chromaffin cells. *PLoS ONE* **8**, 70638. doi:10.1371/journal.pone.0070638

Gulyas-Kovacs, A., de Wit, H., Milosevic, I.,-KOchubey, O., Toonen, R., Klingauf, J., Verhage, M. and Sorensen, J. B. (2007). Munc18-1: sequential interactions with the fusion machinery stimulate vesicle docking and priming. *J. Neurosci.* **27**, 8676-8686. doi:10.1523/JNEUROSCI.0658-07.2007

Han, G. A., Park, S., Bin, N.-R., Jung, C. H., Kim, B., Chandrasegaram, P., Matsuda, M., Riadi, I., Han, L. and Sugita, S. (2014). A pivotal role for pro-335 in balancing the dual functions of Munc18-1 domain-3a in regulated exocytosis. *J. Biol. Chem.* **289**, 33617-33628. doi:10.1074/jbc.M114.584805

He, E., Wierda, K., van Westen, R., Broeke, J. H., Toonen, R. F., Cornelisse, L. N. and Verhage, M. (2017). Munc13-1 and Munc18-1 together prevent NSF-dependent de-priming of synaptic vesicles. *Nat. Commun.* **8**, 15915. doi:10.1038/ncomms15915

Jiao, J., He, M., Port, S. A., Baker, R. W., Xu, Y., Qu, H., Xiong, Y., Wang, Y., Jin, H., Eisemann, T. J. et al. (2018). Munc18-1 catalyzes neuronal SNARE assembly by templating SNARE association. *Elife* **7**, e41771. doi:10.7554/eLife.41771

Kurps, J. and de Wit, H. (2012). The role of Munc18-1 and its orthologs in modulation of cortical F-actin in chromaffin cells. *J. Mol. Neurosci.* **48**, 339-346. doi:10.1007/s12031-012-9775-8

Kurps, J., Broeke, J. H., Cijsouw, T.,-KOmpatscher, A., van Weering, J. R. T. and de Wit, H. (2014). Quantitative image analysis tool to study the plasma membrane localization of proteins and cortical actin in neuroendocrine cells. *J. Neurosci. Methods* **236**, 1-10. doi:10.1016/j.jneumeth.2014.07.022

Lang, T., Wacker, I., Wunderlich, I., Rohrbach, A., Giese, G., Soldati, T. and Almers, W. (2000). Role of actin cortex in the subplasmalemmal transport of secretory granules in PC-12 cells. *Biophys. J.* **78**, 2863-2877. doi:10.1016/S0006-3495(00)76828-7

Lauwers, E., Goodchild, R. and Verstreken, P. (2016). Membrane lipids in presynaptic function and disease. *Neuron* **90**, 11-25. doi:10.1016/j.neuron.2016.02.033

Malacombe, M., Bader, M.-F. and Gasman, S. (2006). Exocytosis in neuroendocrine cells: New tasks for actin. *Biochim. Biophys. Acta Mol. Cell Res.* **1763**, 1175-1183. doi:10.1016/j.bbamcr.2006.09.004

Martin, S., Tomatis, V. M., Papadopulos, A., Christie, M. P., Malintan, N. T., Gormal, R. S., Sugita, S., Martin, J. L., Collins, B. M. and Meunier, F. A. (2013). The Munc18-1 domain 3a loop is essential for neuroexocytosis but not for syntaxin-1A transport to the plasma membrane. *J. Cell Sci.* **126**, 2353-2360. doi:10.1242/jcs.126813

Meijer, M., Dörr, B., Lammertse, H. C., Blithikioti, C., van Weering, J. R. T., Toonen, R. F. G., Söllner, T. H. and Verhage, M. (2018). Tyrosine phosphorylation of Munc18-1 inhibits synaptic transmission by preventing SNARE assembly. *EMBO J.* **37**, 300-320. doi:10.15252/embj.201796484

Meunier, F. A. and Gutiérrez, L. M. (2016). Captivating new roles of F-actin cortex in exocytosis and bulk endocytosis in neurosecretory cells. *Trends Neurosci.* **39**, 605-613. doi:10.1016/j.tins.2016.07.003

Morgan, A. and Burgoyne, R. D. (1997). Common mechanisms for regulated exocytosis in the chromaffin cell and the synapse. *Semin. Cell Dev. Biol.* **8**, 141-149. doi:10.1006/scdb.1996.0133

Munch, A. S., Kedar, G. H., van Weering, J. R. T., Vazquez-Sanchez, S., He, E., Andre, T., Braun, T., Sollner, T. H., Verhage, M. and Sorensen, J. B. (2016). Extension of helix 12 in Munc18-1 induces vesicle Priming. *J. Neurosci.* **36**, 6881-6891. doi:10.1523/JNEUROSCI.0007-16.2016

Neher, E. (2018). Neurosecretion: what can we learn from chromaffin cells. *Pflügers Arch. Eur. J. Physiol.* **470**, 7-11. doi:10.1007/s00424-017-2051-6

Papadopulos, A., Gomez, G. A., Martin, S., Jackson, J., Gormal, R. S., Keating, D. J., Yap, A. S. and Meunier, F. A. (2015). Activity-driven relaxation of the cortical actomyosin II network synchronizes Munc18-1-dependent neurosecretory vesicle docking. *Nat. Commun.* **6**, 1-11. doi:10.1038/ncomms7297

Parisotto, D., Pfau, M., Scheutzow, A., Wild, K., Mayer, M. P., Malsam, J., Sinning, I. and Söllner, T. H. (2014). An extended helical conformation in domain 3a of Munc18-1 provides a template for SNARE (soluble N-ethylmaleimide-sensitive factor attachment protein receptor) complex assembly. *J. Biol. Chem.* **289**, 9639-9650. doi:10.1074/jbc.M113.514273

Porat-Shliom, N., Milberg, O., Masedunskas, A. and Weigert, R. (2013). Multiple roles for the actin cytoskeleton during regulated exocytosis. *Cell. Mol. Life Sci.* **70**, 2099-2121. doi:10.1007/s00018-012-1156-5

Rettig, J. and Neher, E. (2002). Emerging roles of presynaptic proteins in Ca++-triggered exocytosis. *Science* **298**, 781-785. doi:10.1126/science.1075375

Saarikangas, J., Zhao, H. and Lappalainen, P. (2010). Regulation of the actin cytoskeleton-plasma membrane interplay by phosphoinositides. *Physiol. Rev.* **90**, 259-289. doi:10.1152/physrev.00036.2009

Santos, T. C., Wierda, K., Broeke, J. H., Toonen, R. F. and Verhage, M. (2017). Early golgi abnormalities and neurodegeneration upon loss of presynaptic proteins munc18-1, syntaxin-1, or SNAP-25. *J. Neurosci.* **37**, 4525-4539. doi:10.1523/JNEUROSCI.3352-16.2017

Schmitz, S. K., King, C.,-KOrtleven, C., Huson, V., Kroon, T., Kevenaar, J. T., Schut, D., Saarloos, I., Hoetjes, J. P., de Wit, H. et al. (2016). Presynaptic inhibition upon CB1 or mGlu2/3 receptor activation requires ERK/MAPK phosphorylation of Munc18-1. *EMBO J.* **35**, 1236-1250. doi:10.15252/embj.201592244

Shin, W., Ge, L., Arpino, G., Villarreal, S. A., Hamid, E., Liu, H., Zhao, W.-D., Wen, P. J., Chiang, H.-C. and Wu, L.-G. (2018). Visualization of membrane pore in live cells reveals a dynamic-pore theory governing fusion and endocytosis. *Cell* **173**, 934-945.e12. doi:10.1016/j.cell.2018.02.062

Sørensen, J. B., Nagy, G., Varoqueaux, F., Nehring, R. B., Brose, N., Wilson, M. C. and Neher, E. (2003). Differential control of the releasable vesicle pools by SNAP-25 splice variants and SNAP-23. *Cell* **114**, 75-86. doi:10.1016/S0092-8674(03)00477-X

Südhof, T. C. and Rizo, J. (2011). Synaptic vesicle exocytosis. *Cold Spring Harb. Perspect. Biol*. **3**. doi:10.1101/cshperspect.a005637

Tamori, Y., Kawanishi, M., Niki, T., Shinoda, H., Araki, S., Okazawa, H. and Kasuga, M. (1998). Inhibition of insulin-induced GLUT4 translocation by Munc18c through interaction with syntaxin4 in 3T3-L1 adipocytes. *J. Biol. Chem.* **273**, 19740-19746. doi:10.1074/jbc.273.31.19740

Tellam, J. T., Macaulay, S. L., McIntosh, S., Hewish, D. R., Ward, C. W. and James, D. E. (1997). Characterization of Munc-18c and syntaxin-4 in 3T3-L1 adipocytes. Putative role in insulin-dependent movement of GLUT-4. *J. Biol. Chem.* **272**, 6179-6186. doi:10.1074/jbc.272.10.6179

Toonen, R. F. G. and Verhage, M. (2003). Vesicle trafficking: pleasure and pain from SM genes. *Trends Cell Biol.* **13**, 177-186. doi:10.1016/S0962-8924(03)00031-X

Toonen, R. F.,-KOchubey, O., de Wit, H., Gulyas-Kovacs, A.,-KOnijnenburg, B., Sørensen, J. B., Klingauf, J. and Verhage, M. (2006). Dissecting docking and tethering of secretory vesicles at the target membrane. *EMBO J.* **25**, 3725-3737. doi:10.1038/sj.emboj.7601256

Trifaró, J.-M., Rodríguez Del Castillo, A. and Vitale, M. L. (1992). Dynamic changes in chromaffin cell cytoskeleton as prelude to exocytosis. *Mol. Neurobiol.* **6**, 339-358. doi:10.1007/BF02757940

Trifaró, J.-M., Gasman, S. and Gutiérrez, L. M. (2008). Cytoskeletal control of vesicle transport and exocytosis in chromaffin cells. *Acta Physiol.* **192**, 165-172. doi:10.1111/j.1748-1716.2007.01808.x

Verhage, M. and Sørensen, J. B. (2008). Vesicle docking in regulated exocytosis. *Traffic* **9**, 1414-1424. doi:10.1111/j.1600-0854.2008.00759.x

Verhage, M., Ascanio, M. S., Plomp, J. J., Brussaard, A. B., Heeroma, J. H., Vermeer, H., Toonen, R. F., Hammer, R. E., Van Den Berg, T. K., Missler, M. et al. (2000). Synaptic assembly of the brain in the absence of neurotransmitter secretion. *Science* **287**, 864-869. doi:10.1126/science.287.5454.864

Vitale, M. L., Del Castillo, A. R., Tchakarov, L. and Trifaro, J. M. (1991). Cortical filamentous actin disassembly and scinderin redistribution during chromaffin cell stimulation precede exocytosis, a phenomenon not exhibited by gelsolin. *J. Cell Biol.* **113**, 1057-1067. doi:10.1083/jcb.113.5.1057

Vitale, M. L., Seward, E. P. and Trifaró, J.-M. (1995). Chromaffin cell cortical actin network dynamics control the size of the release-ready vesicle pool and the initial rate of exocytosis. *Neuron* **14**, 353-363. doi:10.1016/0896-6273(95)90291-0

Voets, T., Toonen, R. F., Brian, E. C., De Wit, H., Moser, T., Rettig, J., Südhof, T. C., Neher, E. and Verhage, M. (2001). Munc18-1 promotes large dense-core vesicle docking. *Neuron* **31**, 581-591. doi:10.1016/S0896-6273(01)00391-9

Washbourne, P., Thompson, P. M., Carta, M., Costa, E. T., Mathews, J. R., Lopez-Benditó, G., Molnár, Z., Becher, M. W., Valenzuela, C. F., Partridge, L. D. et al. (2002). Genetic ablation of the t-SNARE SNAP-25 distinguishes mechanisms of neuroexocytosis. *Nat. Neurosci.* **5**, 19-26. doi:10.1038/nn783

Wen, P. J., Grenklo, S., Arpino, G., Tan, X., Liao, H. S., Heureaux, J., Peng, S. Y., Chiang, H. C., Hamid, E., Zhao, W. D. et al. (2016). Actin dynamics provides membrane tension to merge fusing vesicles into the plasma membrane. *Nat. Commun*. **7**, 12604. doi:10.1038/ncomms12604